Science
AAAS

# Mussel-Inspired Surface Chemistry for Multifunctional Coatings

Haeshin Lee, *et al.*

*Science* **318**, 426 (2007);
DOI: 10.1126/science.1147241

elements (four cases), LTR elements (five cases), SINEs (six cases) and simple sequences (two cases), and (ii) high complexity regions: SDs (five cases) and unique DNA (five cases). As an interesting example of the latter, we observed a fusion involving the protein-coding regions of two olfactory-receptor (OR) genes, *OR51A4* and *OR51A2*, resulting in a new gene predicted to encode a protein identical to OR51A4, with upstream regions from *OR51A2* (Fig. 5, B and C). *OR51A4* and *OR51A2* are found in the rhesus monkey; their presence confirms that the "ancestral" region contains both genes and that SV formation involved a recent gene-fusion event. We suggest that deviation in gene content for the large OR gene family may lead to diversity of olfactory perception in the human population.

In addition to NHEJ, retrotransposition, and NAHR, other events may have occurred or could not be assigned. In four cases, simple sequence DNA was present at the breakpoint junctions; NAHR or other mechanisms may be involved in their formation (*23*). Four cases were unassigned, and two sequenced SVs closed gaps in the human reference sequence (see, e.g., Fig. 5, B and C).

We also analyzed 14 inversions. Four instances of homologous recombination between inverted repeats (HRIR) were observed; surprisingly, the remaining 10 inversions appeared to involve events that do not require homology. Overall, a large fraction of all of the SVs we sequenced (at least 57%) had one or both breakpoints in nonrepetitive sequence, indicating that high-complexity genomic regions are subject to structural variation.

**Discussion.** PEM enabled global detection of SVs at 3-kb resolution, and an average resolution of breakpoint assignment of 644 bp. We identified ~1300 SVs in two individuals, which suggests that humans may differ to a greater extent in SVs than in SNPs, when considering the total number of nucleotides affected. To date, most human genome–sequencing projects do not directly analyze SVs. Our study reveals that, given their high frequency, it will be essential to incorporate SV detection into human genome–sequencing projects (*24*). Overall, PEM is a cost-effective method both for improving genome assemblies and for revealing SVs present in the genome for a better understanding of human diversity.

PEM has several advantages over existing methods. First, PEM increases resolution of SV detection to the level of confirmation by PCR, and resolution can be further improved by more careful selection of evenly sized DNA fragments for circularization. Second, PEM does not require preparation of a DNA library that involves cloning. However, the short size of fragments (3 kb) used in this study hampers the detection of simple insertions >3 kb, although larger insertions can be detected by their mated ends. Similar to other SV detection methods, a limitation of PEM is that SVs in regions with multiple copies of highly similar and long (>3 kb) repeats are difficult to identify. Fortunately, although 45% of the human genome is composed of high–copy number repeat elements, these are often sufficiently divergent or short and can thus be distinguished by PEM. Additional refinements of PEM are also possible and will eventually allow detection of all SVs in the human genome.

### References and Notes


1. J. Sebat *et al.*, *Science* **305**, 525 (2004).
2. A. J. Iafrate *et al.*, *Nat. Genet.* **36**, 949 (2004).
3. E. Tuzun *et al.*, *Nat. Genet.* **37**, 727 (2005).
4. R. Redon *et al.*, *Nature* **444**, 444 (2006).
5. B. E. Stranger *et al.*, *Science* **315**, 848 (2007).
6. H. Stefansson *et al.*, *Nat. Genet.* **37**, 129 (2005).
7. E. Gonzalez *et al.*, *Science* **307**, 1434 (2005).
8. M. Fanciulli *et al.*, *Nat. Genet.* **39**, 721 (2007).
9. J. R. Lupski, P. Stankiewicz, *PLoS Genet* **1**, e49 (2005).
10. J. L. Freeman *et al.*, *Genome Res.* **16**, 949 (2006).
11. J. O. Korbel *et al.*, *Proc. Natl. Acad. Sci. U.S.A.* **104**, 10110 (2007).
12. Materials and methods are available as supporting material on *Science* Online.
13. M. Margulies *et al.*, *Nature* **437**, 376 (2005).
14. The International HapMap Consortium, *Nature* **437**, 1299 (2005).
15. R. R. Selzer *et al.*, *Genes Chromosomes Cancer* **44**, 305 (2005).
16. A. E. Urban *et al.*, *Proc. Natl. Acad. Sci. U.S.A.* **103**, 4534 (2006).
17. B. P. Coe *et al.*, *Genomics* **89**, 647 (2007).
18. P. M. Kim *et al.*, in preparation, available at http://arxiv.org/abs/0709.4200v1.
19. J. A. Bailey, G. Liu, E. E. Eichler, *Am. J. Hum. Genet.* **73**, 823 (2003).
20. E. V. Linardopoulou *et al.*, *Nature* **437**, 94 (2005).
21. R. E. Mills, E. A. Bennett, R. C. Iskow, S. E. Devine, *Trends Genet.* **23**, 183 (2007).
22. R. Belshaw *et al.*, *J. Virol.* **79**, 12507 (2005).
23. A. Bacolla, R. D. Wells, *J. Biol. Chem.* **279**, 47411 (2004).
24. R. Khaja *et al.*, *Nat. Genet.* **38**, 1413 (2006).


25. We thank C. Turcotte, C. Celone, D. Riches, and 454 colleagues, and R. Bjornson at the Yale High Performance Computation Center (funded by NIH grant: RR19895-02) for technical support. Funding was provided by a Marie Curie Fellowship (J.O.K.), the Alexander von Humboldt Foundation (A.T.), the Wellcome Trust (N.P.C., M.E.H., J.C., and F.Y.), Roche Applied Science, and the NIH (Yale Center of Excellence in Genomic Science grant). Accessions can be found in table S5, and at http://sv.gersteinlab.org/.


### Supporting Online Material

www.sciencemag.org/cgi/content/full/1149504/DC1
Materials and Methods
Tables S1 to S6
Fig. S1
References


21 August 2007; accepted 13 September 2007
Published online 27 September 2007;
10.1126/science.1149504
Include this information when citing this paper.




REPORTS

# Mussel-Inspired Surface Chemistry for Multifunctional Coatings


Haeshin Lee,[1] Shara M. Dellatore,[2] William M. Miller,[2,3] Phillip B. Messersmith[1,3,4]*



We report a method to form multifunctional polymer coatings through simple dip-coating of objects in an aqueous solution of dopamine. Inspired by the composition of adhesive proteins in mussels, we used dopamine self-polymerization to form thin, surface-adherent polydopamine films onto a wide range of inorganic and organic materials, including noble metals, oxides, polymers, semiconductors, and ceramics. Secondary reactions can be used to create a variety of ad-layers, including self-assembled monolayers through deposition of long-chain molecular building blocks, metal films by electroless metallization, and bioinert and bioactive surfaces via grafting of macromolecules.


Methods for chemical modification of bulk material surfaces play central roles in modern chemical, biological, and materials sciences, and in applied science, engineering, and technology (*1–4*). The existing toolbox for the functional modification of material surfaces includes methods such as self-assembled monolayer (SAM) formation, functionalized silanes, Langmuir-Blodgett deposition, layer-by-layer assembly, and genetically engineered surface-binding peptides (*5–9*). Although widely implemented in research, many available methods have limitations for widespread practical use; specific examples include the requirement for chemical specificity between interfacial modifiers and surfaces (e.g., alkanethiols on noble metals and silanes on oxides), the use of complex instrumentation and limitations of substrate size and shape (Langmuir-Blodgett deposition), or the need for multistep procedures for implementation (layer-by-layer assembly and genetically engineered surface-binding peptides).

Development of simple and versatile strategies for surface modification of multiple classes of materials has proven challenging, and few generalized methods for accomplishing this have been previously reported (*10*). Our approach is inspired by the adhesive proteins secreted by

mussels for attachment to wet surfaces (*11*). Mussels are promiscuous fouling organisms and have been shown to attach to virtually all types of inorganic and organic surfaces (*12*), including classically adhesion-resistant materials such as poly(tetrafluoroethylene) (PTFE) (Fig. 1A). Clues to mussels' adhesive versatility may lie in the amino acid composition of proteins found near the plaque-substrate interface (Fig. 1, B to D), which are rich in 3,4-dihydroxy-L-phenylalanine (DOPA) and lysine amino acids (*13*). In addition to participating in reactions leading to bulk solidification of the adhesive (*14*–*16*), DOPA forms strong covalent and noncovalent interactions with substrates (*17*).

DOPA and other catechol compounds perform well as binding agents for coating inorganic surfaces (*18*–*23*), including the electropolymerization of dopamine onto conducting electrodes (*24*); however, coating of organic surfaces has proven much more elusive. Hypothesizing that the coexistence of catechol (DOPA) and amine (lysine) groups may be crucial for achieving adhesion to a wide spectrum of materials, we identified dopamine as a small-molecule compound that contains both functionalities (Fig. 1E). We show that this simple structural mimic of *Mytilus edulis* foot protein 5 (Mefp-5) is a powerful building block for spontaneous deposition of thin polymer films on virtually any bulk material surface and that the deposited films are easily adapted for a wide variety of functional uses.

Simple immersion of substrates in a dilute aqueous solution of dopamine, buffered to a pH typical of marine environments (2 mg of dopamine per milliliter of 10 mM tris, pH 8.5), resulted in spontaneous deposition of a thin adherent polymer film (Fig. 1, F to H). Analysis by atomic force microscopy (AFM) indicated that the polymer film thickness was a function of the immersion time and reached a value of up to 50 nm after 24 hours (Fig. 1G). X-ray photoelectron spectroscopy (XPS) analysis of 25 diverse materials coated for 3 hours or more revealed the absence of signals specific to the substrate (solid red bars in Fig. 1H; see also fig. S1), indicating the formation of a polymer coating of 10 nm or more in thickness. Little variation in the atomic composition of the coating was found (blue circles in Fig. 1H), suggesting that the composition of the polymer coating was independent of the substrate composition. The nitrogen-to-carbon signal ratio (N/C) of 0.1 to 0.13 is similar to that of the theoretical value for dopamine (N/C = 0.125), implying that the coating is derived from dopamine polymerization. Evidence for dopamine polymerization was found through analysis of the modification solution by gel permeation chromatography (fig. S2) and of coated substrates by time-of-flight secondary ion mass spectrometry (TOF-SIMS) (fig. S3). Polymer was found both in solution and on the substrate, with TOF-SIMS clearly revealing signals corresponding to dihydroxyphenyl-containing polymer fragments. Although the exact polymerization mechanism is unknown at this time, it is likely to involve oxidation of the catechol to a quinone, followed by polymerization in a manner reminiscent of melanin formation, which occurs through polymerization of structurally similar compounds (*25*) (fig. S3).

The polydopamine coating is able to form on virtually all types of material surfaces (Fig. 1H): noble metals (Au, Ag, Pt, and Pd), metals with native oxide surfaces (Cu, stainless steel, and NiTi shape-memory alloy), oxides [$TiO_2$, noncrystalline $SiO_2$, crystalline $SiO_2$ (quartz) $Al_2O_3$, and $Nb_2O_5$], semiconductors (GaAs and $Si_3N_4$), ceramics [glass and hydroxyapatite (HAp)], and synthetic polymers {polystyrene (PS), polyethylene (PE), polycarbonate (PC), polyethylene

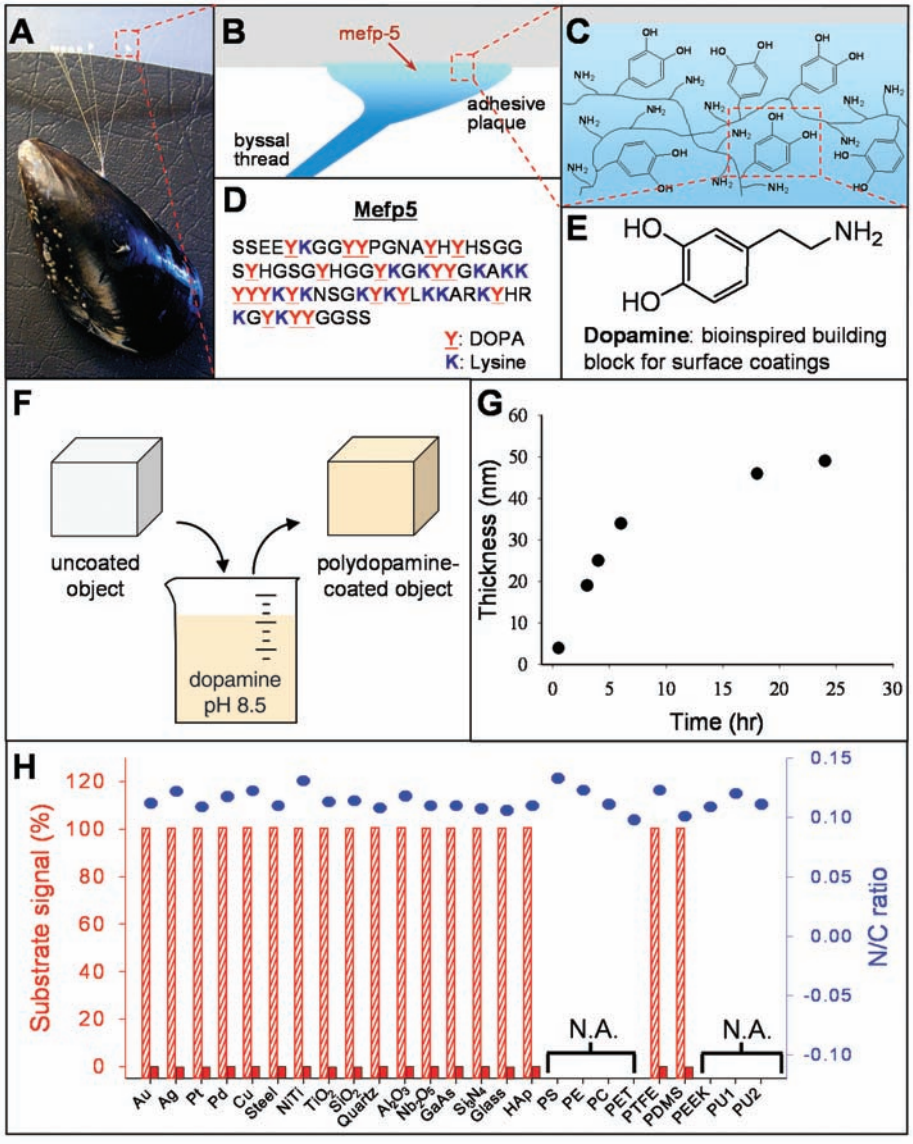


**Fig. 1.** (**A**) Photograph of a mussel attached to commercial PTFE. (**B** and **C**) Schematic illustrations of the interfacial location of Mefp-5 and a simplified molecular representation of characteristic amine and catechol groups. (**D**) The amino acid sequence of Mefp-5 (*13*, *34*). (**E**) Dopamine contains both amine and catechol functional groups found in Mefp-5 and was used as a molecular building block for polymer coatings. (**F**) A schematic illustration of thin film deposition of polydopamine by dip-coating an object in an alkaline dopamine solution. (**G**) Thickness evolution of polydopamine coating on Si as measured by AFM of patterned surfaces. (**H**) XPS characterization of 25 different polydopamine-coated surfaces. The bar graph represents the intensity of characteristic substrate signal before (hatched) and after (solid) coating by polydopamine. The intensity of the unmodified substrate signal is in each case normalized to 100%. Substrates with characteristic XPS signals indistinguishable from the polydopamine signal are marked by "N.A." The blue circles represent the N/C after polydopamine coating (details of XPS data analysis are available in fig. S1 and table S2).

[1]Biomedical Engineering, Northwestern University, 2145 Sheridan Road, Evanston, IL 60208, USA. [2]Chemical and Biological Engineering, Northwestern University, 2145 Sheridan Road, Evanston, IL 60208, USA. [3]Institute for BioNanotechnology in Medicine, Northwestern University, 2145 Sheridan Road, Evanston, IL 60208, USA. [4]Materials Science and Engineering, Northwestern University, 2145 Sheridan Road, Evanston, IL 60208, USA.

*To whom correspondence should be addressed. E-mail: philm@northwestern.edu

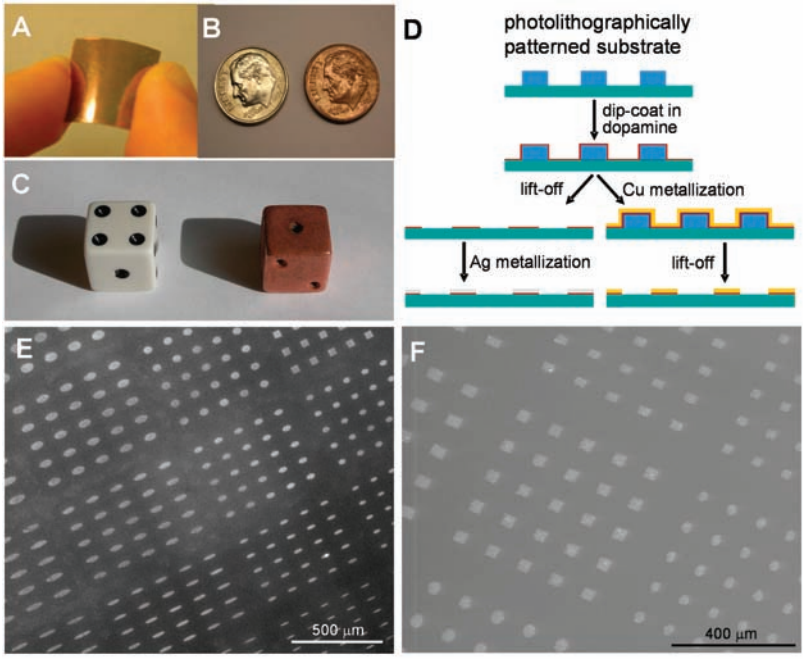


**Fig. 2.** Polydopamine-assisted electroless metallization of substrates. (**A** to **C**) Electroless copper deposition on polydopamine-coated nitrocellulose film (A), coin (B), and three-dimensional plastic object (C). (**D**) Schematic representation of electroless metallization of photoresist-patterned surfaces coated with polydopamine. Photoresist (blue) was removed before silver metallization (left) or after copper metallization (right). (**E** and **F**) Scanning electron microscopy images showing micropatterns of silver on Si (E) and copper on a glass substrate (F).

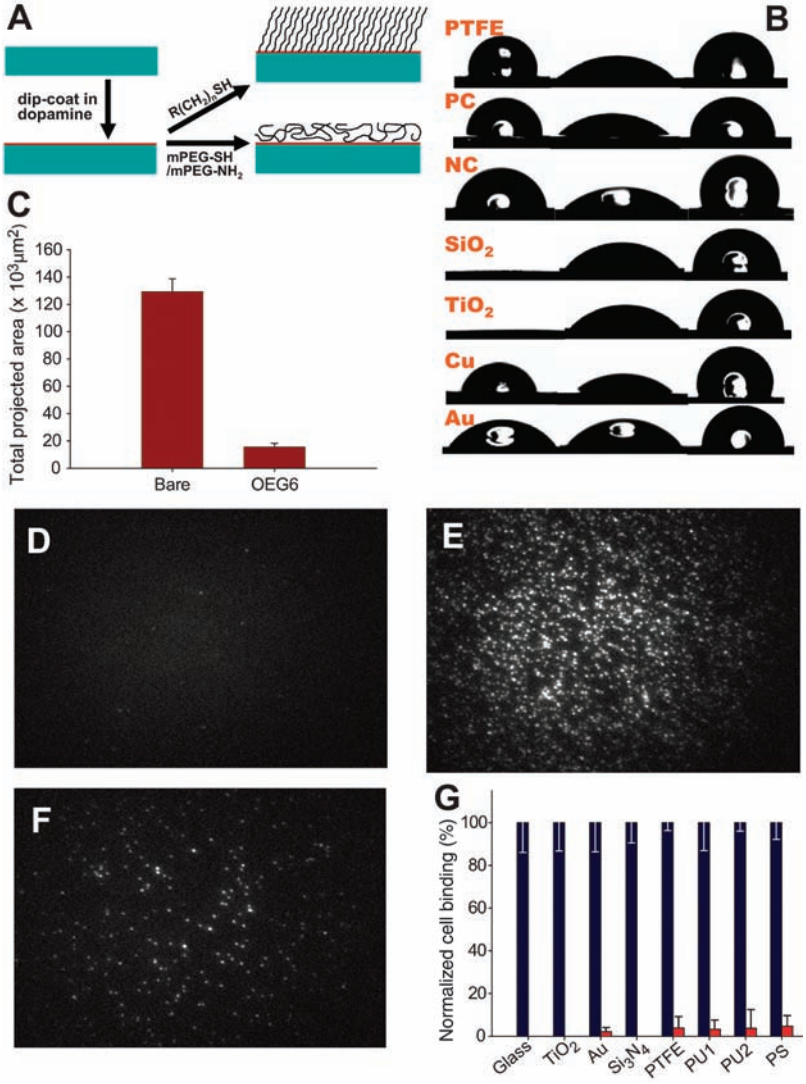


**Fig. 3.** Polydopamine-assisted grafting of various organic molecules. (**A**) Schematic illustration of alkanethiol monolayer (top right) and PEG polymer (bottom right) grafting on polydopamine-coated surfaces. (**B**) Pictures of water droplets on several unmodified (left), polydopamine-coated (middle), and alkanethiol-grafted (right) substrates. Substrates investigated include organic polymers [PTFE, PC, and nitrocellulose (NC)], metal oxides ($SiO_2$ and $TiO_2$), and noble metals (Cu and Au). Contact angle values are shown in table S1. (**C**) NIH 3T3 fibroblast cell adhesion to unmodified glass ("Bare") and OEG6-terminated alkanethiol monolayer formed on polydopamine-coated glass. Error bars indicate SD. (**D** to **F**) Total internal reflection fluorescence (TIRF) microscopy of Cy3-conjugated Enigma homolog protein adsorption to mPEG-$NH_2$–grafted polydopamine-coated glass (48-hour exposure to protein solution) (D), bare glass (30-min exposure) (E), and mPEG-silane immobilized on bare glass (48-hour exposure) (F). (**G**) NIH 3T3 fibroblast cell adhesion to bare surfaces (black) and to polydopamine-coated surfaces after grafting with mPEG-SH (red) (prenormalized data are available in table S3). Error bars indicate SD.

terephthalate (PET), PTFE, polydimethylsiloxane (PDMS), polyetheretherketone (PEEK), and polyurethanes [Carbothane (PU1) and Tecoflex (PU2)]}.

The polydopamine coating was found to be an extremely versatile platform for secondary reactions, leading to tailoring of the coatings for diverse functional uses. For example, the metal-binding ability of catechols (*26*) present in the polydopamine coating was exploited to deposit adherent and uniform metal coatings onto substrates by electroless metallization. This was demonstrated through deposition of silver and copper metal films via dip-coating of polydopamine-coated objects into silver nitrate and copper(II) chloride solutions, respectively (Fig. 2). Metal film deposition was confirmed by XPS and TOF-SIMS analysis, which demonstrated successful metal film deposition on several ceramic, polymer, and metal substrates: nitrocellulose, coinage metals, commercial plastics, $Si_3N_4$, glass, Au, $TiO_2$, $SiO_2$ PC, PS, PEEK, $Nb_2O_5$, $Al_2O_3$, and NiTi (figs. S4 and S5). Metal coatings were successfully applied in this manner to flexible polymer substrates and bulk objects with complex shapes (Fig. 2, A to C), as well as to flat surfaces in which the polydopamine coating had been patterned by means of standard photolithography techniques (Fig. 2, D to F). Unlike many other approaches to electroless metallization (*27*), the use of (immobilized) colloidal metal seed particles was unnecessary for spontaneous formation of adherent metal films. In the case of silver film deposition, the apparent reductive capacity of the polydopamine sublayer was sufficient to eliminate the need for addition of an exogenous reducing agent in the metal salt solution, implying oxidation of the underlying polydopamine layer.

Polydopamine coatings also support a variety of reactions with organic species for the creation of functional organic ad-layers. For example, under oxidizing conditions, catechols react with thiols and amines via Michael addition or Schiff base reactions (*14*, *28*) (fig. S3B). Thus, immersion of polydopamine-coated surfaces into a thiol- or amine-containing solution provided a convenient route to organic ad-layer deposition through thiol- and amine-catechol adduct formation (Fig. 3A). We demonstrated this approach for deposition of organic ad-layers in the form of alkanethiol monolayer, synthetic polymer, and biopolymer coatings.

A monolayer of alkanethiol was spontaneously formed through simple immersion of polydopamine-coated substrates (Fig. 3B). Monolayer formation on the polydopamine sublayer is believed to involve reaction between terminal thiol groups and the catechol/quinone groups of the polydopamine coating, in a manner analogous to the reaction between thiols and noble metal films in the formation of conventional SAMs. Alkanethiol monolayers formed by this approach are likely to contain defects but nevertheless appear to be functionally similar to conventionally formed SAMs. We therefore refer to these monolayers of alkanethiols as "pseudo-SAMs" (pSAMs). For example, spontaneous formation of pSAMs with the use of methyl-terminated alkanethiol (C12-SH) was suggested by water contact angles of greater than 100° (Fig. 3B and table S1) (*29*) and XPS spectra revealing the presence of sulfur in the modified surfaces (fig. S6). pSAMs were formed in this way on at least seven different materials, including several ceramics and polymers.

Through proper choice of secondary reactants, polydopamine coatings can be transformed into surfaces that have specific chemical properties, such as the suppression of nonspecific biological interactions or the promotion of specific ones (*23*, *24*). We first demonstrated this by formation of pSAMs from heterobifunctional molecular precursors on polydopamine-coated surfaces as described above. pSAMs terminated by oligo(ethylene glycol) (OEG6) were found to be largely resistant toward fibroblast cell attachment (Fig. 3C), behaving in a qualitatively similar fashion to nonfouling SAMs formed on gold (*30*).

Grafting of polymer ad-layers onto polydopamine coatings was accomplished through the use of thiol- or amine-functionalized polymers in the secondary reaction step, giving rise to bioresistant and/or biointeractive surfaces. For example, fouling-resistant surfaces were made by covalently grafting amine- or thiol-terminated methoxy-poly(ethylene glycol) [(mPEG-$NH_2$ or mPEG-SH) in 10 mM tris, pH 8.5, 50°C] to the polydopamine-coated surface (fig. S7). mPEG-$NH_2$–modified polydopamine-coated glass exhibited substantial reduction in nonspecific protein adsorption as compared with uncoated glass and also outperformed glass surfaces modified by a silane-terminated PEG in terms of fouling resistance after 2 days of continuous exposure to protein solution (Fig. 3, D to F). Similarly, mPEG-SH grafting onto a variety of polydopamine-coated

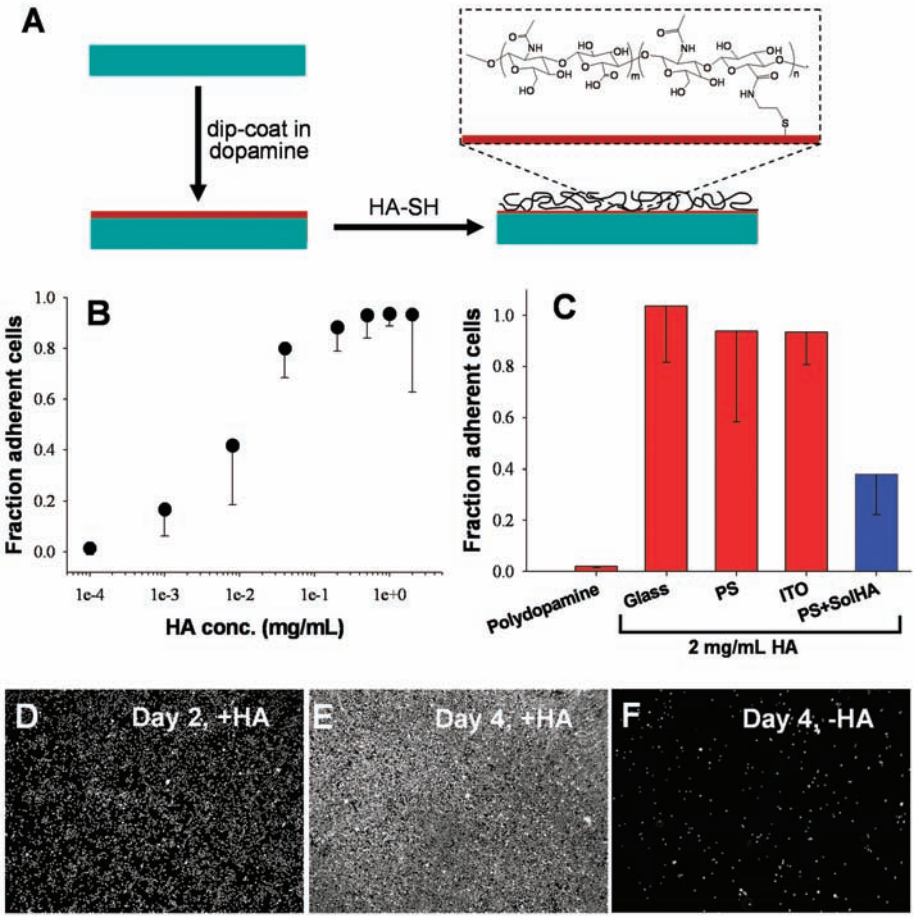


**Fig. 4.** Polydopamine-assisted grafting of a biomacromolecule for biospecific cell interaction. (**A**) Representative scheme for HA conjugation to polydopamine-coated surfaces. (**B**) Adhesion of M07e cells on polydopamine-coated PS increases with the HA solution concentration used during grafting. Error bars indicate SD. (**C**) Bioactive HA ad-layers were formed on polydopamine-coated glass, tissue-culture PS, and indium tin oxide (ITO), as demonstrated by attachment of M07e cells (red bars). Competition with soluble HA (blue bar) confirmed that cell adhesion was due to grafted HA. Error bars indicate SD. (**D** to **F**) Polydopamine-modified PS grafted with HA (0.5 mg of HA per milliliter of 10 mM tris, pH 8.0) retains bioactivity during long-term culture with M07e cells. Images taken after normal-force centrifugation show almost 100% attachment of expanding M07e cells at days 2 [2760 ± 390 cells/cm$^2$ (D)] and 4 [5940 ± 660 cells/cm$^2$ (E)]. In the absence of HA, the polydopamine-coated surface supported similar levels of M07e cell expansion at day 4 but did not support cell adhesion [610 ± 630 cells/cm$^2$ (F)].

substrates led to dramatic reduction of fibroblast cell attachment as compared with the unmodified substrates (Fig. 3G and table S3). The polydopamine coating itself was supportive of fibroblast cell adhesion at a level similar to that of bare substrates {for example, the total area of attached cells on 1.08 $mm^2$ of polydopamine-modified $SiO_2$ [$(46 \pm 1.4) \times 10^3$ $\mu m^2$] was similar to that of unmodified $SiO_2$ [$(55 \pm 8.6) \times 10^3$ $\mu m^2$]}, leading us to conclude that the observed decrease in cell adhesion was due to the grafted mPEG-SH.

Finally, we engineered polydopamine surfaces for specific biomolecular interactions by forming an ad-layer of the glycosaminoglycan hyaluronic acid (HA). HA/receptor interactions are important for physiological and pathophysiological processes, including angiogenesis, hematopoietic stem cell commitment and homing, and tumor metastasis (*31*, *32*). Partially thiolated HA (*33*) was grafted onto a variety of polydopamine-coated substrates (Fig. 4), and HA ad-layer bioactivity was measured via adhesion of the human megakaryocytic M07e cell line. Unlike fibroblasts, M07e cells did not adhere to polydopamine but did adhere to HA-grafted polydopamine surfaces in a dose-dependent manner (Fig. 4B). Together with decreased binding in the presence of soluble HA (Fig. 4C), these findings are consistent with expression of the HA receptor CD44 by M07e cells (fig. S8). Polydopamine and HA-grafted polydopamine surfaces were biocompatible, as evidenced by similar levels of M07e cell expansion as compared with cell expansion on tissue-culture PS surfaces, although only the HA-grafted polydopamine surfaces supported cell adhesion (Fig. 4, D to F, and fig. S9).

We introduced a facile approach to surface modification in which self-polymerization of dopamine produced an adherent polydopamine coating on a wide variety of materials. Polydopamine coatings can, in turn, serve as a versatile platform for secondary surface-mediated reactions, leading ultimately to metal, SAM, and grafted polymer coatings. This two-step method of surface modification is distinctive in its ease of application, use of simple ingredients and mild reaction conditions, applicability to many types of materials of complex shape, and capacity for multiple end-uses.

### References and Notes


1. B. D. Ratner, A. S. Hoffman, Eds., *Biomaterials Science: An Introduction to Materials in Medicine* (Elsevier Academic, San Diego, CA, ed. 2, 2004).
2. J.-H. Ahn *et al.*, *Science* **314**, 1754 (2006).
3. P. Alivisatos, *Nat. Biotechnol.* **22**, 47 (2004).
4. R. Langer, *Science* **293**, 58 (2001).
5. J. C. Love, L. A. Estroff, J. K. Kriebel, R. G. Nuzzo, G. M. Whitesides, *Chem. Rev.* **105**, 1103 (2005).
6. G. Decher, *Science* **277**, 1232 (1997).
7. G. Roberts, Ed. *Langmuir-Blodgett Films* (Plenum, New York, 1990).
8. S. R. Whaley, D. S. English, E. L. Hu, P. F. Barbara, A. M. Belcher, *Nature* **405**, 665 (2000).
9. C. Tamerler, M. Sarikaya, *Acta Biomater.* **3**, 289 (2007).
10. D. Y. Ryu, K. Shin, E. Drockenmuller, C. J. Hawker, T. P. Russell, *Science* **308**, 236 (2005).
11. J. H. Waite, M. L. Tanzer, *Science* **212**, 1038 (1981).
12. G. A. Young, D. J. Crisp, in *Adhesion*, K. W. Allen, Ed. (Applied Science, London, vol. 6, 1982).
13. J. H. Waite, X. X. Qin, *Biochemistry* **40**, 2887 (2001).
14. L. A. Burzio, J. H. Waite, *Biochemistry* **39**, 11147 (2000).
15. M. J. Sever, J. T. Weisser, J. Monahan, S. Srinivasan, J. J. Wilker, *Angew. Chem. Int. Ed.* **43**, 448 (2004).
16. M. Yu, J. Hwang, T. J. Deming, *J. Am. Chem. Soc.* **121**, 5825 (1999).
17. H. Lee, N. F. Scherer, P. B. Messersmith, *Proc. Natl. Acad. Sci. U.S.A.* **103**, 12999 (2006).
18. M. Yu, T. J. Deming, *Macromolecules* **31**, 4739 (1998).
19. J. L. Dalsin, B.-H. Hu, B. P. Lee, P. B. Messersmith, *J. Am. Chem. Soc.* **125**, 4253 (2003).
20. A. R. Statz, R. J. Meagher, A. E. Barron, P. B. Messersmith, *J. Am. Chem. Soc.* **127**, 7972 (2005).
21. T. Paunesku *et al.*, *Nat. Mater.* **2**, 343 (2003).
22. C. Xu *et al.*, *J. Am. Chem. Soc.* **126**, 9938 (2004).
23. S. Zürcher *et al.*, *J. Am. Chem. Soc.* **128**, 1064 (2006).
24. Y. Li, M. Liu, C. Xiang, Q. Xie, S. Yao, *Thin Solid Films* **497**, 270 (2006).
25. W. Montagna, G. Prota, J. A. Kenney Jr., *Black Skin: Structure and Function* (Academic Press, San Diego, CA, 1993).
26. C. G. Pierpont, C. W. Lange, *Prog. Inorg. Chem.* **41**, 331 (1994).
27. M. Charbonnier, M. Romand, G. Stremsdoerfer, A. Fares-Karam, *Recent Res. Dev. Macromol. Res.* **4**, 27 (1999).
28. M. J. LaVoie, B. L. Ostaszewski, A. Weihofen, M. G. Scholssmacher, D. J. Selkoe, *Nat. Med.* **11**, 1214 (2005).
29. P. E. Laibinis *et al.*, *J. Am. Chem. Soc.* **113**, 7152 (1991).
30. K. L. Prime, G. M. Whitesides, *J. Am. Chem. Soc.* **115**, 10714 (1993).
31. D. N. Haylock, S. K. Nilsson, *Regenerat. Med.* **1**, 437 (2006).
32. B. P. Toole, *Nat. Rev. Cancer* **4**, 528 (2004).
33. H. Lee, S. H. Choi, T. G. Park, *Macromolecules* **39**, 23 (2006).

34. Single-letter abbreviations for the amino acid residues are as follows: A, Ala; C, Cys; D, Asp; E, Glu; F, Phe; G, Gly; H, His; I, Ile; K, Lys; L, Leu; M, Met; N, Asn; P, Pro; Q, Gln; R, Arg; S, Ser; T, Thr; V, Val; W, Trp; and Y, Tyr.

35. This research was supported by NIH grants DE 14193 and HL 74151. The authors thank T. G. Park and H. Lee for donation of thiolated HA, N. F. Scherer and X. Qu for their generous discussion and technical assistance with TIRF microscopy, and K. Healy for photomask donation. This research used the NUANCE characterization facilities (Keck II, EPIC, and NIFTI) at Northwestern University.


### Supporting Online Material

www.sciencemag.org/cgi/content/full/318/5849/426/DC1
Materials and Methods
Figs. S1 to S10
Tables S1 to S3
References


2 July 2007; accepted 12 September 2007
10.1126/science.1147241


# Structure of a Thiol Monolayer–Protected Gold Nanoparticle at 1.1 Å Resolution


**Pablo D. Jadzinsky,[1,2]* Guillermo Calero,[1]* Christopher J. Ackerson,[1]† David A. Bushnell,[1] Roger D. Kornberg[1]‡**



Structural information on nanometer-sized gold particles has been limited, due in part to the problem of preparing homogeneous material. Here we report the crystallization and x-ray structure determination of a *p*-mercaptobenzoic acid (p-MBA)–protected gold nanoparticle, which comprises 102 gold atoms and 44 p-MBAs. The central gold atoms are packed in a Marks decahedron, surrounded by additional layers of gold atoms in unanticipated geometries. The p-MBAs interact not only with the gold but also with one another, forming a rigid surface layer. The particles are chiral, with the two enantiomers alternating in the crystal lattice. The discrete nature of the particle may be explained by the closing of a 58-electron shell.


Nanometer-size metal particles are of fundamental interest for their chemical and quantum electronic properties and of practical interest for many potential applications (*1*, *2*). With the development of facile routes of synthesis (*3*), gold nanoparticles coated with surface thiol layers have been studied in most detail. The particles are typically heterogeneous as synthesized, and though their size distribution may be narrowed by fractionation or other means (*4*–*9*), no atomically monodisperse preparation has been reported, and no atomic structure has been obtained. Electron microscopy (EM) (*10*, *11*), powder x-ray diffraction (PXRD) (*12*), and theoretical studies have led to the idea of Marks decahedral (MD) and truncated octahedral geometries of the metal core, with crystalline packing and {111} faces (*13*). According to this idea, discrete core sizes represent "magic numbers" of gold atoms, arising from closed geometric shells (*14*). Alternatives of amorphous (*15*), molten, or quasimolten (*16*) cores have also been proposed. The structure of the surface thiol layer is similarly obscure. The nature of the gold-sulfur interaction (*17*), the fate of the sulfhydryl proton (*18*), and the conformation of the organic moiety all remain to be determined. The thiols are


[1]Department of Structural Biology, Stanford University School of Medicine, Stanford, CA 94305, USA. [2]Department of Applied Physics, Stanford University, Stanford, CA 94305, USA.

*These authors contributed equally to this work.
†Present address: Department of Chemistry and Biochemistry, University of Colorado, Boulder, CO 80309, USA.
†Present address: Department of Chemistry and Biochemistry, University of Colorado, Boulder, CO 80309, USA.
‡To whom correspondence should be addressed. E-mail: kornberg@stanford.edu